

# Short, Powerful, and Agile Current Drivers for Magnetic Resonance

LAZAR SHTIRBERG, AHARON BLANK

*Schulich Faculty of Chemistry, Technion – Israel Institute of Technology, Haifa 32000, Israel*

**ABSTRACT:** A system for the generation of short, powerful, and agile pulses of current drive is described. The system is made of several submodules, most of them ‘home-made’ and is capable of producing current pulses ranging from 9 A for 150 ns pulses to 94 A for 1400 ns pulse duration, when connected to a nominal  $0.6 \Omega/2.75 \mu\text{H}$  coil. The amplitude of successive current pulses can be updated in the  $\sim\mu\text{s}$  time scale. Such capabilities are very useful in the field of electron spin resonance microimaging and for the measurements of diffusion by electron spin resonance. A variant of the system can also be used for the nuclear magnetic resonance imaging of samples located in grossly inhomogeneous magnetic field or for solid-state nuclear magnetic resonance imaging. Details of the system electronic design as well as some representative experimental results are provided. © 2011 Wiley Periodicals, Inc. Concepts Magn Reson Part B (Magn Reson Engineering) 39B: 119–127, 2011

**KEY WORDS:** ESR; EPR; NMR; imaging; gradients

## I. INTRODUCTION

Many experimental methods in the field of magnetic resonance make use of fast, powerful, and agile current drivers. These include techniques such as nuclear magnetic resonance imaging (MRI) (1), as well as the less known but still useful electron spin resonance (ESR) imaging (2). Another such technique is pulsed gradient spin echo (PGSE), which is used in connection with both NMR (3) and ESR (4, 5), field jump methods (6) and pulsed ultra high magnetic field NMR and ESR spectroscopy (7, 8). The prevalence and importance of these methods has led to the development of a wide arsenal of means to provide appropriate current drives in response to well-defined

experimental requirements. In MRI, for example, state-of-the-art drivers can supply more than 500 A with a voltage drive of up to 2000 V and slew rates of more than  $1 \text{ A}/\mu\text{s}$  going into coils having inductance of up to 1 mH (9). Furthermore, in most MRI applications a very low current ripple of  $\sim 1\%$  or less is required but gradients strength is limited to no more than  $\sim 1 \text{ T/m}$ . In the field of NMR microscopy and PGSE NMR, where coils are much smaller, state-of-the-art drivers can provide up to 120 A of current (10) with slew rates also in the  $1 \text{ A}/\mu\text{s}$  region which combine with efficient gradient coils can achieve gradients of up to  $50 \text{ T/m}$  (11). The minimal duration of the current pulse in these and similar NMR experiments is in the  $\sim 1\text{-ms}$  time scale.

The field of ESR is characterized by very different time scales with common  $T_2$  values in the microsecond and submicrosecond range. As a result, most of the experiments in ESR imaging that are conducted by continuous wave and pulsed techniques employ constant and not pulsed gradients (12, 13). There are, however, many advantages to the use of pulsed rather than fixed gradients, such as lower power deposition in the gradient coils, narrower bandwidth for excita-

Received 26 January 2011; revised 13 March 2011; accepted 21 April 2011

Correspondence to: Aharon Blank; E-mail: ab359@tx.technion.ac.il  
Concepts in Magnetic Resonance Part B (Magnetic Resonance Engineering), Vol. 39B(3) 119–127 (2011)

Published online in Wiley Online Library (wileyonlinelibrary.com).  
DOI 10.1002/cmr.b.20199

© 2011 Wiley Periodicals, Inc.

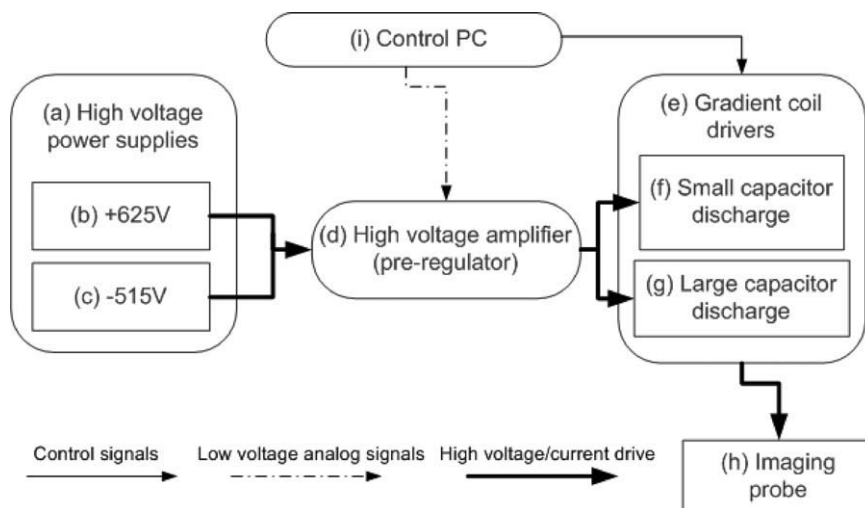


**Figure 1** Block diagram of the pulsed current driver system.

tion and data acquisition, faster image acquisition, and the possibility of observing diffusion with PGSE and related sequences. Furthermore, as noted, pulsed currents can also be used for field jump experiments, which are very important in distance measurement by ESR (6). In view of the above, there have been many efforts in the past to perform experiments with pulsed magnetic fields having short rise and fall times. Starting with the pioneering work of Tsvetkov and co-workers on pulsed ESR imaging (14), there are several examples of the development and use of fast pulsed current drives. In the early 1990s, Freed's ESR group developed a pulsed current driver system for ESR imaging (15). The driver was designed to provide rectangular pulses with peak currents of up to 60 A, having rise and fall times of  $\sim 50$  ns when feeding gradient coil with an inductance of  $0.2 \mu\text{H}$  (resulting in maximum gradient amplitude of slightly less than 1 T/m). In parallel, Conradi et al. took advantage of the fact that in many types of experiments the exact shape (as opposed to the integral) of the current pulse is of no importance. (Examples of these are pulses for phase gradients in imaging and for PGSE pulse sequences.) They came up with a simplified design that provided pulses of  $\sim 3.8 \mu\text{s}$ , with a peak current of 13 A going into coils with inductance of  $3.2 \mu\text{H}$ , leading to a gradient peak amplitude of  $\sim 0.2$  T/m in their configuration (16). The basic principle behind their design is charging a capacitor and then discharging it into the gradient coil. This produces a rather clean and intense half-sine current pulse.

Following this early work, many improvements to this approach were carried out in the lab of Kaplan (2) and later again in the lab of Freed, leading to the

production of larger currents, shorter pulses, and more intense gradients (17). The most recent version of such drivers is based on a similar idea but is much more powerful and enables currents ranging from 9 A for 150 ns pulses to 94 A for 1400 ns pulse duration when connected to a nominal  $0.6 \Omega/2.75 \mu\text{H}$  coil (18). These pulses produce gradients of up to 500 T/m in miniature coils used for ESR microimaging and ESR-PGSE experiments. In this article, we present in detail the design and performance of this latest version of pulsed gradient drivers.

## II. THE PULSED CURRENT DRIVER SYSTEM

The overall block diagram of the gradient driver system is shown in Fig. 1. It is comprised of two commercial high voltage power supplies (Lambda GEN600-2.6), each with an output of 1.5 kW having voltages of +625 and  $-515$  V (items (b) and (c) in the drawing). The reason for this slight asymmetry in power sources is due to component limitations. While MOSFETS and transistors for positive supply with favorable characteristics are available for +600 V, components for negative supply are limited to  $\sim -500$  V. These supplies feed a high voltage amplifier (d) that also receives an analog output from the computer (differential 0 to  $\pm 5$  V) and amplifies it by a factor of 60 (for the positive output) and 50 (for the negative output). The importance of this unit is that it can vary the voltage rapidly and stabilize it on the required value, thus providing the necessary agile response of the system to gradient drive stepping up/down. This pre-regulated voltage is used to feed the

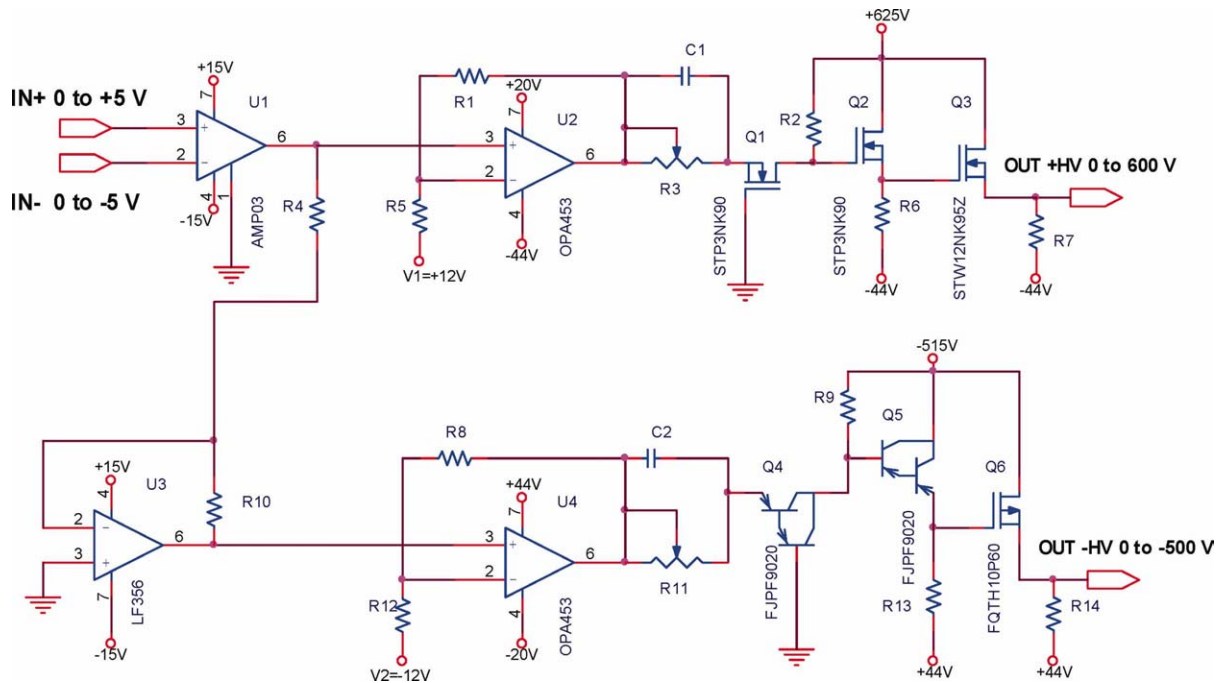


Figure 2 Electronic schematic of the high voltage amplifier.

capacitor charge/discharge units [items (f) and (g) in the drawing], which are the heart of the gradient coil driver system. Let us now describe in more detail the “home-made” components of this system, which are the high voltage amplifier (pre-regulator) and the gradient drivers units.

### High Voltage Amplifier (Pre-regulator)

The electronic schematic of the high voltage amplifier is provided in Fig. 2. This unit can supply a current of up to 10 A and change its output voltage from 0 to +600 V (or -500V) in a few microseconds, according to a differential analog input voltage from the computer (0 to  $\pm 5$  V). Input voltage goes through two gain amplifier units, one with a 0 phase and the other (in the lower part of the schematic) with a phase of  $180^\circ$  going to the negative arm of the amplifier. Following that, both positive and negative voltages go into operational amplifiers with a gain of  $\sim 3$  to 4. The supply bias voltage of  $\pm 12$  V for these two amplifiers must be very stable because any error here would be amplified by the full gain of the system (60 for the positive voltage and 50 for the negative voltage). The positive and negative voltage currents proceed through a MOSFET (for the positive voltage) and Darlington transistor (for the negative voltage), which serve as protection preventing the output’s high voltage from going back to the computer’s ana-

log output card. The last two stages have a gain of  $\sim 15$  and are made of two MOSFETs (Darlington transistors for the negative voltage), with the first one having very low junction capacitance to enable the agile response of the system. Resistors  $R_3$  and  $R_{11}$  can be modified to provide zero voltage bias (nominally less than  $\pm 300$  mV).

### Gradient Coil Drivers

The electronic schematic of one of the gradient coil drivers is provided in Fig. 3. This unit operates by first charging a capacitor (one of the capacitors  $C_1$  to  $C_{12}$  - see later) and then discharging it into the gradient coil ( $L_1$ ). Each capacitor (selectable by a manual rotary switch) provides a different pulse length for the resulting half-sine current pulse, according to the equation:

$$T_{\text{pulse}} = \pi\sqrt{LC} \quad [1]$$

Two similar capacitor are charged simultaneously, one of them connected to the positive voltage (through “switch+ charge 1” or “switch+ charge 2”) and the other to the negative voltage (through “switch- charge 1” or “switch- charge 2”). Control of charge duration and selection between switches 1 and 2 is performed digitally by the control PC (see Fig. 1). The reason for having two possible capaci-

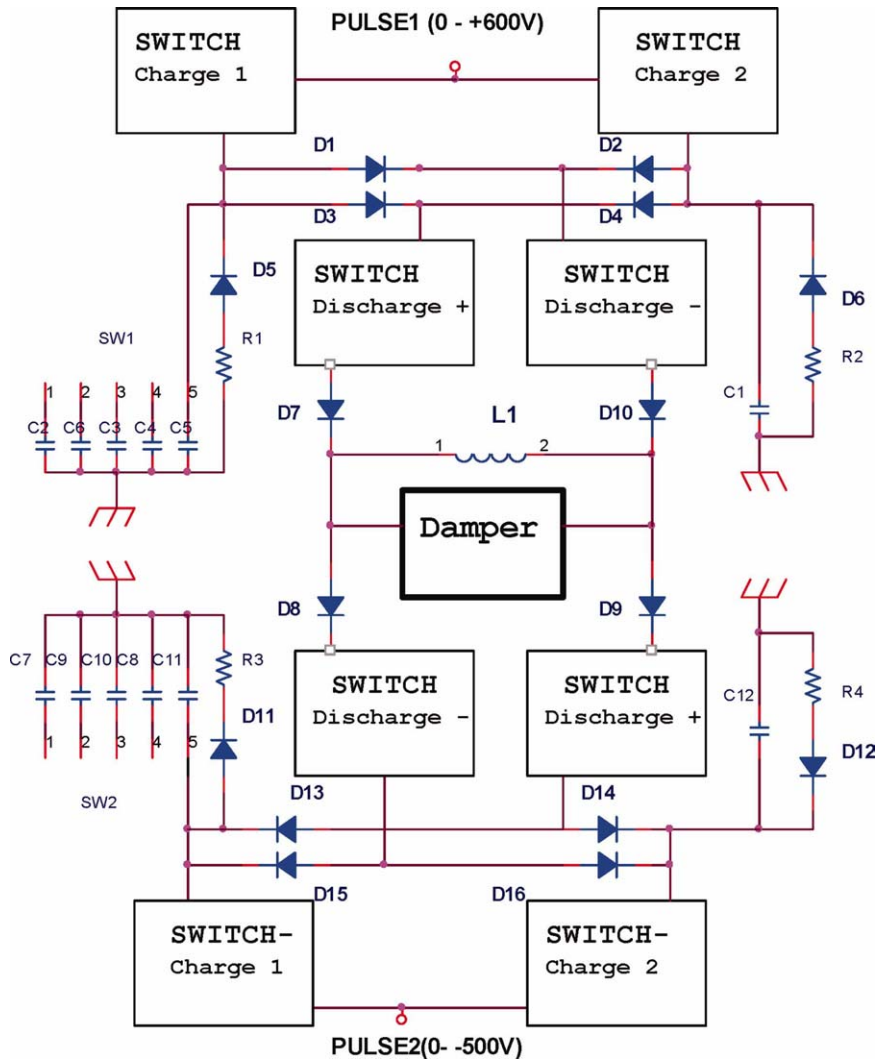
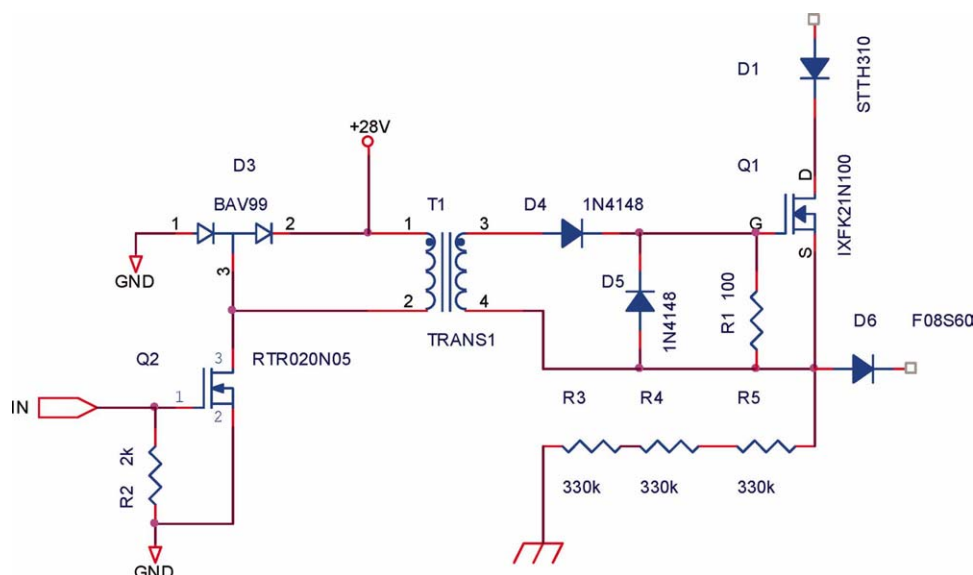


Figure 3 Electronic schematic of the gradient coil driver.

tors (1 and 2) as a charging option will be explained later. Following the charging period, which can take  $\sim 5$  to  $20 \mu\text{s}$ , depending on the size of the capacitor, the system is ready for discharging the capacitors into the gradient coil. This again is done by computer-controlled switches, which are activated in pairs (“Discharge +” or “Discharge -”). The Discharge + pair provides a path for the discharge current in one direction while the Discharge - provides a path in the opposite direction. This facilitates the use of bi-polar gradient fields that are required in phase-encoded imaging experiments. A typical high voltage switch module is shown in Fig. 4. It has a digital input from the computer that triggers a low voltage fast MOSFET that charges (through an isolating transformer) the gate of a high-voltage/high-current MOSFET. The diodes  $D_1$ - $D_4$  and  $D_{13}$ - $D_{16}$  ensure the right direction of the

current’s path and prevents a breakdown of the MOSFET at high voltage.

A very important feature of this gradient driver is its short “dead time” following the end of the half-sine pulse. This means that absolutely no current can flow in the circuit after the pulse ends. Such residual current can be due to parasitic capacitance in the circuit or switch imperfections. The elimination of current after the gradient pulse is achieved by two complementary methods. First, as noted earlier, there are two types of charge capacitors available for selection by the computer. The reason for this is that at low charge voltage values (up to  $\sim 30 \text{ V}$ ) the high voltage switches do not behave very well and the current pulses tend to be much longer than the nominal value based on Eq. [1]. The alternative charge capacitors (shown on the right in Fig. 3) are much smaller than the capacitor required for the nominal pulse length



**Figure 4** Electronic schematic of a typical high voltage switch module, which is part of the gradient coil driver.

and peak currents needed for a given experiment. This means that the pulse length involving this alternative capacitor is much shorter. During the imaging sequence the computer can automatically select the small capacitor at low gradient values, thereby eliminating most of the problems mentioned earlier regarding low voltage MOSFET operation. This is because the use of a small capacitor with a relatively high charge voltage but a short pulse duration is equivalent (in terms of the gradient integral) to that of a large capacitor with a small charge voltage and a long pulse duration (but the latter has the residual current problem at low charge voltage). A second complementary approach for eliminating unwanted current in times longer than the required nominal gradient-pulse length is the use of a damper circuit connected to the coil in the manner shown in Fig. 3. The electronic schema of this damper circuit is shown in Fig. 5. This circuit receives a digital input from the computer a few hundreds of nanoseconds after the discharge pulse trigger (depending on the discharge capacitor's size and the required pulse length). The digital pulse activates a MOSFET that drives another two high voltage MOSFETs through an isolating transformer that effectively shunts the coil and dumps out all the residual current in it after the nominal end of the pulse.

### III. RESULTS

As noted in Section I earlier, the pulsed current driver system has been used in the generation of phase encoding gradients in ESR microimaging

experiments, reaching resolutions that are better than 400 nm (18). It was also employed in the first diffusion measurements of paramagnetic species in liquid solutions by PGSE-ESR (5, 19). Here we will not describe these and other related results but rather concentrate on the performance of the driver system itself in terms of peak current, pulse duration, dead time, and agility.

The first set of results describes the performance of the high voltage amplifier (pre-regulator) unit. As noted earlier, the purpose of this unit is to provide an agile, computer-controlled, high voltage source to charge the capacitors located in the gradient coil driver unit. One of the most important features of the high voltage amplifier unit is the capability to change its output voltage relatively rapidly. This is very useful because in imaging experiments one must step up or down the gradient amplitude and this means changes in the capacitor's charge voltage. In ESR, fast coverage of the image "k-space" can be achieved with a  $T_1$ -limited rate (typically a few microseconds); therefore, the amplifier's output voltage must be able to change and stabilize in this time scale. Figure 6 shows typical results measured for the high voltage amplifier unit, demonstrating its fast rise and fall times to a varying voltage drive from the computer. In this case the voltage was stepped almost instantaneously at time zero from 0 to  $\pm 5$  V in the differential input drive of the unit (coming out of the computer, see Fig. 2). It is apparent that after  $\sim 10$  to 15  $\mu$ s the voltage is stabilized both in the positive and negative polarity outputs. The drive of the high volt-



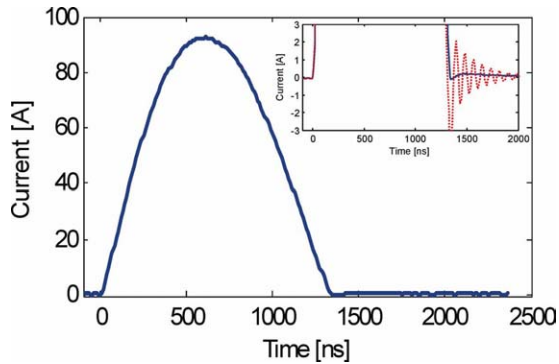


**Figure 8** The same as Fig. 7 but for discharge capacitor of 40  $\mu\text{F}$ .

slope ( $dV/dt$ ) of “real life capacitors” to approximately 250–500  $\text{V}/\mu\text{s}$  for the film capacitors employed in our system. The maximum current amplitude observed is  $\sim 9.5$  A. This can be compared to the theoretical value, calculated using the following equation (18):

$$I_{\max} \approx V_{\text{charge}} \sqrt{\frac{C}{L + \pi R \sqrt{LC}}} \quad [2]$$

which gives  $\sim 13$  A for the present experimental conditions. The value in the experiment is lower probably due to loss of energy into parasitic capacitance and other ohmic components in the system. Figure 8 provides the experimental results for the other end of the system performance, using charge capacitors of 80 nF for the positive and negative charge voltages (i.e. equivalent serial capacitance of 40 nF). Here the measured pulse duration is 1,400 ns, compared to the theoretical value of 1,050 ns. The maximum current is  $\sim 94$  A, compared to the theoretical value of 120.6 A. Again, we suspect that changes in the static and dynamic resistance of the MOSFETs and/or the non-linear behavior of the capacitors under fast voltage changes, together with their being “pushed” into a regime of very high voltage/current, are the source for the deviation from the simplified theoretical values we presented. The inserts in Figs. 7 and 8 show also the effect of the damper circuit on the trailing edge of the pulse. The solid line shows the current with the damper circuit and the dashed line is without the damper circuit. It is clear that without the damper there is much “ringing” due to energy that accumulates in parasitic capacitance and continues to be charged/discharged by and into the coil. It should be noted that measuring very small currents after such a powerful pulse is a difficult task even with modern

scopes. In many cases we have found that while the scope measurements show no residual current after the gradient pulse, in practice the ESR imaging or PGSE experiments reveal to us the existence of some “leftovers” that cannot be ignored (5, 19). For example, in PGSE-ESR one seeks to find a perfect cancellation of phase gradients by two consecutive gradient pulses, and postpulse residual currents limit the fidelity of such cancellation and degrade the quality of the echo signal recovery. This echo signal recovery is therefore a very sensitive indicator for current existence just after the gradient pulse. In ESR microimaging we have found in previous cases that if there are residual currents after the phase gradient pulse, the size of the image (resolution) depends slightly on the value of  $\tau$  (the  $\pi/2$ – $\pi$  interpulse distance in a Hahn echo imaging pulse sequence). This is because for larger values of  $\tau$  the integral of the gradient pulses is a bit larger. The present generation of pulsed gradient systems, as presented in this work, showed a very good performance under such “ESR imaging and PGSE tests.” This included mainly the acquisition of images with Hahn echo series using phase gradients with varying values of  $\tau$ , where we have found out that because of the good and fast cut-off of the gradient pulse the resolution is identical for all values of  $\tau$  and images can be superimposed on top of each other and analyzed correctly [for example, to obtain pixel-wise amplitude and  $T_2$  values (20)]. With these experiments we found out that for a nominal gradient pulse, which measured on the scope to be 250 ns long, one can apply  $\tau$  as small as 280 ns and still get artifact-free images and  $\tau$  independent resolution. This implies a gradient pulse “dead time” of less than 30 ns.

Another important feature of the system is its pulse repetition rate. As noted earlier, the charging voltage can be varied very quickly, and a typical variation from one  $k$ -space value to another (requiring typically only a few volts of change in the charge voltage) can be achieved in a few microseconds (based on the characteristics of the high voltage amplifier – see Fig. 6). However, to complement the picture one must also consider the time it takes for the capacitor to charge after each pulse. Figure 9 shows the voltage on the positive voltage charge capacitor (medium value of 10 nF – corresponding to equivalent capacitance of 5 nF for both positive and negative capacitors when connected in series) and the current pulse produced. It can be seen that it takes  $\sim 10$   $\mu\text{s}$  to charge the capacitor, if one starts from a completely discharged one. The charge time is limited by the available current in the output of the high voltage amplifier. For charge capacitor values with equiva-

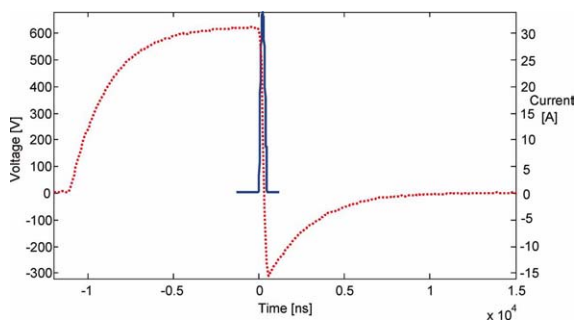


**Figure 9** The voltage measured on a charge capacitor of 10 mF during the charge/discharge process (dotted line) along with the current pulse produced by the system (solid line and vertical scale on the right).

lent capacitance of up to 5 nF a repetition rate of up to 40 kHz is possible. For larger capacitors with equivalent capacitance of up to 40 nF, the repetition rate is limited to  $\sim 20$  kHz. Figure 9 also shows the discharge current pulse and the voltage on the capacitor during discharge.

#### IV. FINAL REMARKS AND CONCLUSIONS

A system for the generation of intense short current pulses for MR experiments was presented here in detail. The system can be used for applications in the field of pulsed ESR imaging and measurement of diffusion by PGSE ESR. A variant of this system, working with coils with higher inductance and using larger charge capacitors, can also be useful for solid-state NMR imaging experiments and for measurements carried out in grossly inhomogeneous magnetic fields (21) As noted in the introduction, in principle, as the pulse duration increases, one can have much higher peak currents in the pulse (up to a certain limit of length/magnitude, of course). Furthermore, it is much easier to provide strong current pulses with short duration as the coil inductance decreases. These facts make it difficult to directly compare the system shown here with other systems described in the literature. One possible figure of merit to the capability of a pulsed current driver system is its “current/pulse duration ratio” for a given coil inductance. (Keeping in mind that this ratio is strongly dependent on the reciprocal of the coil inductance and thus applying it as a figure of merit is valid over only a limited range of driven coil inductance.) The system shown here, employed with a coil inductance of 2.8  $\mu\text{H}$ , provides one of the highest current/pulse duration ratio we are aware of, reaching values of  $6.9 \times 10^7$ . This should be compared to no

more than  $\sim 10^6$  in state-of-the-art NMR systems, but they often use coils with inductance in the range of tens and hundreds of  $\mu\text{H}$ . Other drivers, developed for ESR, achieved a current/pulse duration ratio of up to  $\sim 6 \times 10^8$ , but with coil inductance of  $\sim 0.5 \mu\text{H}$ . We prefer to work with coils having an inductance larger than  $\sim 1.5 \mu\text{H}$  to make them dominant over the inductance of a typical  $\sim 50$ -cm transmission line that can reach  $\sim 0.5 \mu\text{H}$ . The bottom line of our design is that, when the current driver system is employed in conjunction with miniature gradient coils, one can achieve gradients of up to 500 T/m over regions of  $\sim 1$  to 2 mm in size (18). To the best of our knowledge these numbers are by far the largest pulsed gradient values described in the literature of magnetic resonance up to date. Furthermore, the short dead time of the system and its relative simplified design add to its usefulness and uniqueness.

#### ACKNOWLEDGMENTS

This work was supported by grant 213/09 from the Israeli Science Foundation, grant 2009401 by the United States-Israel Binational Science Foundation, by grant 201665 from the European Research Council (ERC), and by the Russell Berrie Nanotechnology Institute at the Technion.

#### REFERENCES

- Bernstein MA, King KF, Zhou ZJ. 2004. Handbook of MRI pulse sequences. Boston: Academic Press.
- Feintuch A, Alexandrowicz G, Tashma T, Boasson Y, Grayevsky A, Kaplan N. 2000. Three-dimensional pulsed ESR fourier imaging. *J Magn Reson* 142:382–385.
- Stejskal EO, Tanner JE. 1965. Spin diffusion measurements—spin echoes in presence of a time-dependent field gradient. *J Chem Phys* 42:288–292.
- Tashma T, Alexandrowicz G, Kaplan N, Dormann E, Grayevsky A, Gabay A. 1999. Restricted electron motion in 1D organic conductors: PGSE-ESR in (PE)2PF6 and (FA)2PF6. *Synth Met* 106:151–155.
- Blank A, Talmon Y, Shklyar M, Shtirberg L, Harneit W. 2008. Direct measurement of diffusion in liquid phase by electron spin resonance. *Chem Phys Lett* 465:147–152.
- Dubinskii AA, Grishin YA, Savitsky AN, Mobius K. 2002. Submicrosecond field-jump device for pulsed high-field ELDOR. *Appl Magn Reson* 22:369–386.
- Wosnitza J, Bianchi AD, Freudenberger J, Haase J, Hermannsdorfer T, Kozlova N, et al. 2007. Dresden

- pulsed magnetic field facility. *J Magn Magn Mater* 310:2728–2730.
8. Ohta H, Okubo S, Sakurai T, Goto T, Kirita K, Ueda K, et al. 2001. High-frequency ESR measurements using pulsed magnetic fields in Kobe. *Physica B: Condensed Matter* 294:624–629.
  9. Sabate J, Garces L, Szczesny P, Qiming Li, Wirth WF. 2005. Applied Power Electronics Conference and Exposition, Twentieth Annual IEEE, Austin, TX 2:1087–1091.
  10. Galvosas P, Stallmach F, Seiffert G, Karger J, Kaess U, Majer G. 2001. Generation and application of ultra-high-intensity magnetic field gradient pulses for NMR spectroscopy. *J Magn Reson* 151:260–268.
  11. Wright AC, Bataille H, Ong HH, Wehrli SL, Song HK, Wehrli FW. 2007. Construction and calibration of a 50 T/m z-gradient coil for quantitative diffusion microimaging. *J Magn Reson* 186:17–25.
  12. Yamada KI, Murugesan R, Devasahayam N, Cook JA, Mitchell JB, Subramanian S, et al. 2002. Evaluation and comparison of pulsed and continuous wave Radiofrequency electron paramagnetic resonance techniques for in vivo detection and imaging of free radicals. *J Magn Reson* 154:287–297.
  13. Eaton GR, Eaton SS, Ohno K. 1991. *EPR Imaging and In Vivo EPR*. Boca Raton: CRC Press.
  14. Milov AD, Pusep AY, Dzuba SA, Tsvetkov YD. 1985. Electron-spin echo as a method of electron-spin-resonance tomography. *Chem Phys Lett* 119:421–425.
  15. Ewert U, Crepeau RH, Dunnam CR, Xu DJ, Lee SY, Freed JH. 1991. Fourier-transform electron-spin-resonance imaging. *Chem Phys Lett* 184:25–33.
  16. Conradi MS, Garroway AN, Cory DG, Miller JB. 1991. Generation of short, intense gradient pulses. *J Magn Reson* 94:370–375.
  17. Blank A, Dunnam CR, Borbat PP, Freed JH. 2004. Pulsed three-dimensional electron spin resonance microscopy. *Appl Phys Lett* 85:5430–5432.
  18. Shtirberg L, Twig Y, Suhovoy E, Levit M, Blank A. 2011. High-sensitivity Q-band electron spin resonance imaging system with submicron resolution. *Rev Sci Instrum* 82:043708.
  19. Talmon Y, Shtirberg L, Harneit W, Rogozhnikova OY, Tormyshev V, Blank A. 2010. Molecular diffusion in porous media by PGSE ESR. *Phys Chem Chem Phys* 12:5998–6007.
  20. Halevy R, Tormyshev V, Blank A. 2010. Micro-imaging of oxygen concentration near live photosynthetic cells by electron spin resonance. *Biophys J* 99:971–978.
  21. Blank A, Ish-Shalom S, Shtirberg L, Zur Y. 2009. Ex situ endorectal MRI probe for prostate imaging. *Magn Reson Med* 62:1585–1596.